Drag Force on a Confined Particle: Particle Transport

Mounia Makhoul, Philippe Beltrame, Maminirina Joelson

Abstract: The hydrodynamic interaction between a channel confinement and a suspended body is an important class of hydrodynamic problems. In this paper, we point out a quantitative study of the effects of the channel boundaries on the drag force exerted by the fluid on the particle surface. As results, we can obtain the drag coefficient as well as the flow in the channel due to the presence or the motion of the particle. We consider a channel with a periodic variation in diameter in which an axisymmetric particle is translating along its axis. Our numerical resolution is performed using the boundary integral formulation of Stokes flow which is solved using a boundary elements method. The numerical results are presented for the cases of spherical and ellipsoidal particles. Different geometric effects like the curvature of the channel, the particle geometry, and the channel size to particle size ratio are handled. Using the second law of Newton, these results enable us to study the existence and kinds of the mechanisms allowing the transport of the suspended particle and experienced by the computed drag force.

Key-Words: Spherical and ellipsoidal particle; Periodic channel; Confined geometry; Drag force; Boundary elements method; Singular integrals.

I. INTRODUCTION

Microfluidic flows past solid particles are encountered in many engineering and biological applications, including motion of blood cells in microvessels and separation of molecules across biological and porous membranes, equally the particle transport in porous media which is of interest in filtration systems. Because of this important applications, substantial research works have been devoted to the study of flows past rigid bodies in one hand, and in another hand the hydrodynamic force experienced by the suspended body. In addition recent works focus on the force exerted on objects immersed in confined geometries. It is well known that particle-channel interactions as well as particle-fluid interactions have effects on the particle motion. For a proper description of a particle behavior in the microfluidic devices, the particle drag force has to be well understood. The studies of such a force has grown out the classical work of Stokes for a translating rigid sphere in an infinite flow. Practically, there is many factors affecting on the particle drag force, as the particle and the channel geometry as good as the particle to channel size ratio: the channel boundaries have a strong impact on the particle force. For this special case, this paper propose a numerical computation of the drag force exerted on an asymmetric particle of arbitrary shape suspended in a fluid flow. The flow occurs in a confined axisymmetric periodic channel. This formulation would be applied for particles and channels of arbitrary geometry and size. The present work was motivated by a micropumping system [16] through periodic micropores channel. Recently [17] showed the role of the force drag in the existence of the particle transport. The model in [17] applies only in the case of fairly small particles. Our study aims at determining the validity of the latter model depending on the particle size and at presenting a generalization for arbitrary particle sizes.

In the past, modeling Stokes force on solid particles suspended in fluid flow was carried out with different analytical and numerical approaches. To determine the characteristics of an unconfined flow around tandem square cylinders in steady and unsteady periodic laminar flow, the authors of [20] have investigated the drag force exerted

on the both cylinders. Using the method of perturbations, Brenner has calculated the Stokes resistance of a rigid particle with arbitrary geometric form suspended in a quasi-static flow, supposed quite at infinity [1], in a shear flow [2], and in an arbitrary initial field flow [3]. The authors of [4] studied numerically by the Lattice-Boltzmann method the boundaries effect on the Stokes force of a sphere, undergoing a uniform translation motion outside the axis of revolution of the cylinder. Their numerical results agree with the experimental results obtained by Ambari [8], who proved that the force is minimal when the particle is on the axis of the cylinder and it increases quickly when the sphere approaches its boundaries. In addition, Happel and Byrne in [9], have discussed the force, the torque and the pressure rise generated by the presence or the motion of a spherical particle or a periodic suspension of spherical particles in a cylindrical duct. Moreover and despite the fact that ellipsoidal particles have a large importance, a major part of the literature has focused only on spherical ones. Blaser in [6], used the analytical formulas developed by [4] and [5] to examine the drag force exerted on small ellipsoidal particles immersed in either a constant, simple shear, two dimensional straining or axisymmetric straining flows. Obviously, only simplified situations are tractable with analytical results. Other authors has concentrated also on the computation of the hydrodynamic force exerted on a moving particle. In an extension of their earlier works motivated by applications in biomechanics, Chen and Skalak in [25] computed the force applied on a file of prolate and oblate spheroidal particles oriented along the axis of a circular tube.

According to that, for more general configuration one should investigate numerical approaches to compute the drag force. The present study deals with spherical and ellipsoidal particles settling in an arbitrary channel form, filled with a viscous fluid flow at a very low Reynolds number, as long as the size of the particle is comparable to the size of the duct.

In order to solve problems in fluid-solid interactions, various numerical methods could be employed. Some authors use the finite element method as in [22], the immersed boundary method as in [23] and the boundary integral equation. This latter exists in several forms expressing (a) the velocity [13], (b) the traction [24], and (c) the pressure [13], as an integral on the boundary surface of the velocity and the traction. This method is based on the viscous hydrodynamic potential theory introduced by Ladyzhenskaya starting from the Greens theorem results. The boundary integral method is particularly suited to solve Stokes flows with complex geometries.

Over the last three decades, the method was widely developed and matured. For instance, Kohr in [7] gave a boundary integral formulation to calculate the perturbation of an infinite incident flow in the presence of a solid sphere and a viscous drop, Jeffrey *et al.* [8], applied such formulation to compute the disturbance velocity field of a Poiseuille flow due to the presence of a sphere. Recently, a numerical-analytical for the boundary elements method is reported in [19] for elliptic problems and aiming at reducing the computation time. In order to compute the Stokes flow, in a quiescent fluid-filled tube of an arbitrary geometry, and due to the presence or motion of a rigid particle, Pozrikidis in [12] has evaluated the force and torque exerted on the particle. His numerical studies were accomplished using the boundary integral formulation.

In the rest of the paper we are going to introduce a formulation of the boundary integral equation describing the problem, then a special treatment for singular integral will be examined, and finally we present some numerical results.

II. MODELLING AND NUMERICAL RESOLUTION

A. Problem Presentation

We consider an incompressible viscous flow through a confining axisymmetric tube past a solid axisymmetric particle. One tube is constituted with some interconnected identical pores with periodic variation in diameter as shown in figure 1. We are interested notably in such pores because they represent some kinds of realistic porous media [16].

The channel has a sinusoidal variation in radius, such as:

$$r(z) = \frac{r_{min}}{2}\left[\sigma + 1 + (\sigma - 1)\cos(2\pi z/L)\right] \quad (1)$$

where L is the pore length, σ the ratio r_{max}/r_{min} called curvature of the pore. Note that $\sigma \geq 1$ and $\sigma = 1$ corresponds to a uniform cylindrical tube.

In this study, we deal with an incompressible quasi-static flow induced by a pressure gradient,

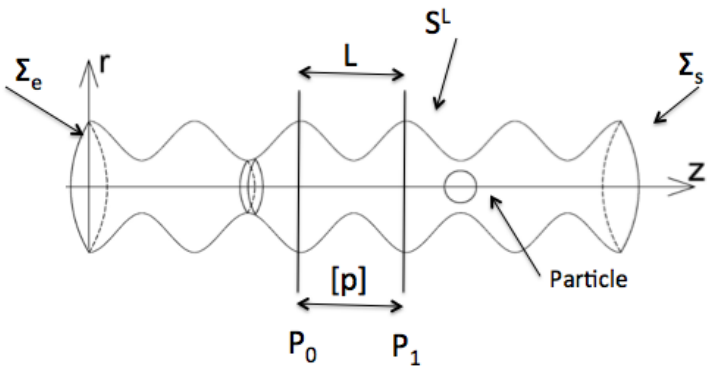

Figure 1: Sketch of the problem: a particle moves in the periodic pore series along the axis. The pore profile is given by the equation (1).

periodically pumped back and forth. Indeed, considering the following characteristic values: the pore length L which is about 10μm, the mean velocity U_m =L/T, where T is the pumping period ranging from 10^{-4} s to 10^{-2}, then the Reynolds number of a fluid as water is small. Therefore, it is a creeping flow described by the Stokes equation and the continuity equation. Moreover, because the fluid is viscous, we consider the no-slip boundary condition. In the following, we work with dimensionless variables. The lengths are scaled by the pore length L, the time by the pumping frequency T and the pressure by the pressure difference $[p]$ imposed by the pumping. Thereby, the Stokes equations describing the problem are:

$$-\vec{\nabla}p + \frac{[p]T}{\eta}\Delta\vec{u} = 0 \tag{2}$$

$$\vec{\nabla}.\vec{u} = 0 \tag{3}$$

For more simplicity, the dimensionless coefficient $\frac{[p]T}{\eta}$ is considered equal to one. We note that one could compute the drag for any desired values of $[p]$, T, and η just by multiplying the dimensionless drag by the latter coefficient. Due to the motion linearity, to compute the drag force, we calculate firstly the velocity and pressure fields (u^0, p^0) without particle and secondly, the perturbation (u^d, p^d) due to a single particle. As in [16], we consider a large number of pores, so that the incident velocity flow u^0 can be assumed periodic. Then, if the pressure $[p]$ is given between the inlet and the outlet of the pore, there is a unique solution of the following problem:

$$-\vec{\nabla}\vec{p^0} + \Delta\vec{u^0} = 0 \tag{4}$$

$$\vec{\nabla}.\vec{u^0} = 0 \tag{5}$$

The boundary conditions are given by the non-slip condition on the lateral surface S^L of the channel, and the periodicity between the two ends,

$$\begin{aligned} \vec{u}^0 &= 0 \text{ on } S^L \\ \vec{u}^0(r,0) &= \vec{u}^0(r,1) \end{aligned} \tag{6}$$

The perturbed flow $(\vec{u}^d, p^d)$ due to the particle is governed by the equations (4) and (5) with the boundary conditions:

$$\begin{aligned} \vec{u}^d &= 0 \text{ on } S^L, \forall z \in [0,L] \\ \vec{u}^d(r,0) &= u^d(r,L) = 0, \ \forall r \\ \vec{u}^d &= u_p - u^0 \text{ on } S_p \end{aligned} \tag{7}$$

Because of the symmetry about the longitudinal axis of the channel, the cylindrical coordinates are chosen for the numerical description.
Owing to the fact of linearity, the associated drag force, $\vec{F}$, acting on the particle may be decomposed into two parts,

$$\vec{F} = \vec{F_1} + \vec{F_2} \tag{8}$$

where $\vec{F_1}$ is the contribution of the initial and non disturbed flow and $\vec{F_2}$ is due to the effect of the perturbed flow. The first term may be written as following:

$$\vec{F_1} = \int_{S_p} \bar{\bar{\sigma}}.\vec{n} \ \mathrm{dS} \tag{9}$$

where $\bar{\bar{\sigma}}$ denotes the stress tensor exerting on the surface of the particle and $\vec{n}$ is the unit normal vector pointing out of the fluid:

$$\bar{\bar{\sigma}} = -p\bar{\bar{\mathbf{I}}} + (\vec{\nabla}u + \vec{\nabla}u^T) \tag{10}$$

Using the Green formula and since the incident fluid is at equilibrium, one can show that the force $\vec{F_1}$ vanishes. In contrast, the second component $\vec{F_2}$ does not vanish. This latter would be also written as a sum of two contributions again because of linearity argument. The first one emphasizes the influence of the particle motion in the fluid, and the second one reveals the effect of the incident flow. In other words, the perturbed problem will be solved as the sum of two problems with different boundary conditions on the particle surface. Firstly we take $u^d = u_p$ (moving particle in a fluid at rest), and secondly u^d = -u^0

(steady particle in a moving fluid). This decomposition allows us to write $\vec{F_2}$ as following:

$$\vec{F_2} = -\gamma(z)\left(u_p - U_{eq}(z)\right)\vec{e}_z \qquad (11)$$

where z designates the position of the particle center, and the $\gamma(z)$ represents the coefficient of the drag force exerted on the particle. The both coefficients $\gamma(z)$ and $U_{eq}(z)$ can be computed after the solution for the boundary traction $\vec{t}$ and simultaneously the velocity $\vec{u}$ have been found. We note that the formulation (11) generalizes the classical expression of the Stokes force which is justified in the case of the non confined flows for particles whose radius is quite small compared to that of the duct.

B. Boundary integral representation

The primary objective of the present work is to compute the both coefficients $\gamma(z)$ and $U_{eq}(z)$ appearing in the formula (11).The starting point, is to find the incident flow through the channel without the presence of the particle, given by (u^0, p^0) while the second point is to compute the disturbance field defined by (u^d, p^d). These both arise as solutions of the Stokes equations and verify the boundary conditions (6) and (7). In order to simplify notations in which follows, we omit the upper-script. Recalling that the flow occurs at small Reynolds number, then the incident velocity field as well as the disturbance velocity field may be described with the integral representation of the Stokes flow:

$$u_k(\vec{x}) = \int_{\partial\Omega} t_i(y)U_i^k(\vec{x},\vec{y}) - u_i(\vec{y})T_i^k(\vec{x},\vec{y}) \quad (12)$$

where $\vec{t}$ and $\vec{u}$ represent the traction and velocity vectors respectively. Having $\vec{t} = \bar{\bar{\sigma}}.\vec{n}$ together with Eq. $(A.)$, we can express the cylindrical components (t_r, t_z) of $\vec{t}$ in function of the pressure and the velocity gradient

$$\begin{pmatrix} t_r \\ \\ t_z \end{pmatrix} = \begin{pmatrix} \Big(-p + 2\partial_r u_r\Big)n_r + \Big(\partial_z u_r + \partial_r u_z\Big)n_z \\ \\ \Big(\partial_z u_r + \partial_r u_z\Big)n_r + \Big(-p + 2\partial_z u_z\Big)n_z \end{pmatrix} \qquad (13)$$

T_i^k and U_i^k designate respectively the stress and velocity tensors associated to the elementary solution called Stokeslet and are given by:

$$U_i^k(\vec{x},\vec{y}) = \frac{1}{8\pi|\vec{y}-\vec{x}|}[\delta_{ik} + \frac{(y_i - x_i)(y_k - x_k)}{|\vec{y}-\vec{x}|^3}] \quad (14)$$

$$T_i^k(\vec{x},\vec{y}) = -\frac{3}{4\pi}\frac{(y_i - x_i)(y_j - x_j)(y_k - x_k)}{|\vec{y}-\vec{x}|^5}.n_j(\vec{y}) \quad (15)$$

where δ_{ik} is the Kronecker's delta. Physically, $U_i^k(\vec{x},\vec{y})$ and $T_i^k(\vec{x},\vec{y})$ are respectively the i^{th} velocity and traction components at the point $\vec{y}$ due to a point force of unit strength located at the point $\vec{x}$ pointing in the k^{th} direction. More detailed informations on boundary integral formulation for Stokes flow and its associated elementary solution can be found in [13, 14]. We note that the terms of U_i^k and T_i^k are singular as $|\vec{y}-\vec{x}|^{-1}$ and $|\vec{y}-\vec{x}|^{-2}$ respectively. The equation (12) can be properly used for $\vec{x}$ inside the pore domain and not on the boundaries. A regularized form of equation (12), which involves only weak singular integrals may be found in [13, 14] and is therefore valid for all $\vec{x}$ located on the boundaries:

$$\int_{\partial\Omega}\left(u_i(\vec{y}) - u_i(\vec{x})\right)T_i{}^k(\vec{x},\vec{y}) - t_i(\vec{y})U_i{}^k(\vec{x},\vec{y})\ \text{dSy} \quad (16)$$

The numerical procedure to compute $\gamma(z)$ and $U_{eq}(z)$ involves the following steps:

1. Problem without the particle: it is supposed to be periodic, thus the pressure difference, $[p]$, is constant between the two ends of the pore.
   - Computation of the velocity profile and the traction at the inlet and on the lateral surface of the channel using equation (16).
   - Computation of the velocity field using equation (12) inside the channel in order to have the incident flow on the particle surface.
2. Assume that far from the particle (in particular at the both ends of the channel) the flow is not disturbed.
3. Assume on one side the boundary condition of the disturbance flow $u^d = u_p$ and compute $\gamma(z)$ and on another side that $u^d = -u_0$ and compute $U_{eq}(z)$ using (16).

A standard method of computing the unknowns appearing above requires a discretization of the channel surfaces: Σ_e, Σ_s S^L and the particle surface S_p into boundary elements, as well as a discretization of the unknowns into nodal values. Then enforcing the integral representation at collocation points leads to a linear system of equations.

C. Numerical implementation

In order to implement the resolution of the first numerical procedure given above the traction vector on Σ_s, $\vec{t^s}$, is expressed in function of the traction on Σ_e, $\vec{t^e}$, as following,

$$\begin{pmatrix} t_r^s(r,z) \\ \\ t_z^s(r,z) \end{pmatrix} = \begin{pmatrix} -t_r^e(r,z) \\ \\ -t_z^e(r,z) + [p] \end{pmatrix}$$

According to these assumptions, the analytical form of t_z^e as a function of the pressure is also constant at $z = 0$. Since the pressure is only defined up an arbitrary constant then without loss of generality we set t_z^e=0. Nevertheless we prove that the radial velocity is equal to zero on the two ends, thereby the unknowns that we should compute at the first step are u_z^e, t_r^e, t_z^L, and t_r^L where t_z^L and t_r^L are respectively the cylindrical components of the traction vector on S^L.
Next, we discretize the two ends of the channel into $2 \times N_1$ boundary elements: $\Sigma_e = \cup_{e=1}^{e=N1} E_e$, $\Sigma_s = \cup_{e=1}^{e=N1} E_e$ and its lateral surface into N_2 boundary elements: $S^L = \cup_{e=1}^{e=N2} E_e$, and we write the boundary integral equation (12) as a sum of elementary integrals. Since the problem is 3D axisymmetric, our boundary elements are curved and defined by two nodes. Then we approximate the unknown vectors on the boundary, it gets the formalism of the finite elements method and leads to calculate the unknowns at the so called interpolation points. For convenience, we choose the points of geometric discretization for interpolation. For each point, N_k of these points, we associate an interpolation function $M_k(y)$, then we write an approximation of order 1 of the unknowns as:

$$u_i(y) = M_k(y)u_i(y^k) + M_{k+1}(y)u_i(y^{k+1}) \quad \text{if } y \in [y^k, y^{k+1}] \quad (17)$$

where $u_i(y^k)$, for k=1,..,$N_e + 1$, are the $N_e + 1$ nodal values that we are going to compute.
Finally, a collocation method is introduced in order to build the discretized problem. The stability of the collocation method is improved in [21]. It consists on forcing the equation (12) to be verified at the set of collocation points, $\vec{x}$, resulting a linear system of form $AX = B$. It is necessary to have at least equations as much as unknowns, so the simplest case is to choose the interpolation points as points of collocation from which the square linear system appearing below will be derived:

$$\begin{pmatrix} E_e & E_e & E_l & E_l \\ L_e & L_e & L_l & L_l \\ E_e & E_e & E_l & E_l \\ L_e & L_e & L_l & L_l \end{pmatrix} \cdot \begin{pmatrix} t_r^e \\ u_z^e \\ t_z^L \\ t_r^L \end{pmatrix} = [p] \begin{pmatrix} B_p \end{pmatrix}$$

where:

- E_e is a $N_1 \times N_1$ end surfaces influence matrix, E_l is a $N_1 \times N_2$ inlet surface-lateral surface influence matrix, L_e is a lateral surface-end surfaces influence matrix, and L_l is lateral surface self influence matrix.
- The second term of the left hand side of the system corresponds to the unknown vector holding the cylindrical components of the velocity and traction fields on the one end and the lateral surface of the channel. It is a $2 \times N_1$+$2 \times N_2$-dimensional vector.
- The term of the right hand side, B_p, is a $2 \times N_1$+$2 \times N_2$-dimensional vector. It reveals integrals over the outlet surface multiplied by the pressure difference $[p]$.

According to the channel geometry, there is a corner connecting Σ_e and S^L and supporting two nodal values, each one attached to the regular portion of the surface and adjacent to the geometric singularity. In this case we add to the final linear system an equation involving the continuity of the traction vector across the corner:

$$t^i.n^j = t^j.n^i \quad (18)$$

Once the above system has been solved, we can compute the velocity of the incident flow over the particle surface using (12). Therefore, we could be able to compute the drag on the particle surface. Its numerical implementation will be performed in the same way as we have explained above. The particle surface is discretized into N_3 boundary elements, then the unknown traction is a $2 \times N_3$-dimensional vector.
Figure 3 presents an example of the computation of the traction field on the lateral surface of the channel due to the incident flow, also the perturbed traction caused by the motion of the sphere. Even though the problem without the particle is periodic, note that the traction is not periodic. In fact, it is due to the presence of the decreasing pressure term in the expression (13) of the traction.

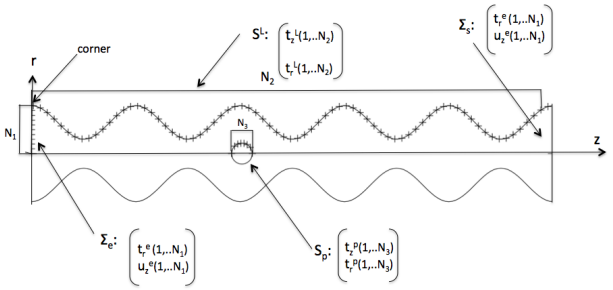

Figure 2: Discretization of the surfaces of the channel and the particle. The two ends of the channel are discretized with $N_1 = 30$ elements, the lateral surface with $N_2 = 150$ elements. The particle surface is discretized with $N_3 = 15$ elements. The elements are straight with two nodes each one. The stress and velocity components on the channel boundaries are approximated with functions of order 1. The traction components on the particle surface are approximated with constant functions.

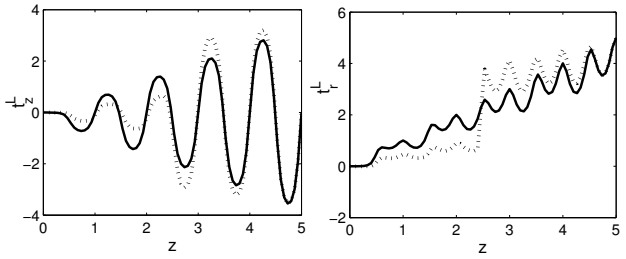

Figure 3: Graph of the (z-component) of the stress vector (left hand side) and the (r-component) (right hand side) on the lateral surface of the channel without the particle (solid line) and with the presence of the particle (dotted line). This result corresponds to a particle localized in the middle of the channel.

Equation (16) involving the traction and the velocity fields on the channel and particle surfaces, allows us to compute the velocity of the flow through the channel past the particle. Our numerical results are consistent with the asymptotic case of the Poiseuille's flow in a cylindrical duct $(\sigma = 1)$. The results concerning the drag and the equivalent velocity are pointed out in the section IV..

One have to note that the elements of the influence matrices are elementary integrals, among which there exist regular integrals, when $\vec{x}$ is not in $[y^k, y^{k+1}]$, and singular ones, when $\vec{x}$ belongs to $[y^k, y^{k+1}]$. Regular integrals are computed using the gauss quadrature formulas. Otherwise, a specific method is introduced in the next section III..

III. SINGULAR INTEGRALS TREATMENT

An elementary integral is singular when $\vec{x}$ belongs to the boundary element of integration. In the past, a plethora of works have been done to treat the singular integrals. We choose the approach developed by Guiggiani *et al.*[15] which has the advantage to be quite generic. The use of the regularized equation of (12), given in [13, 14] allows us to deal only with weak singular integrals.

The technique to calculate the weak singular integrals is based on the introduction of a polar system coordinates, (ρ,α), centered at the singular point, or the collocation point. Note that the cylindrical coordinates (r, θ, z) do not match the polar coordinates tangent to the pore surface. Using the Taylor expansion, we can show that the square of the distance d between two collocation points and the integration point can be written as following:

$$d^2(z,\theta) = \rho^2(z,\theta) + o(\rho^2(z,\theta)) \qquad (19)$$

where $\rho(z,\theta)$ is:

$$\rho(z,\theta) = \sqrt{(1 + H(z_c)^2)(z - z_c))^2 + (r(z_c)\theta)^2} \qquad (20)$$

The function $r(z)$ appearing in (20) designates the pore radius, H its derivate. (z,θ) are the cylindrical coordinates of the integration point, and (z_c,θ=0) are those of the collocation point. The equation (20) helps us to perform the following change of variables :

$$(1 + H(z_c)^2)(z - z_c) = \rho\cos\alpha \qquad (21)$$

$$(r(z_c)\theta) = \rho\sin\alpha \qquad (22)$$

The main idea of this method is to isolate the singular kernel of U_i^k tensor and expresses it with the new variables ρ and α, it is a kind of Laurent series:

$$U_i{}^k(z,\theta) = \frac{f(\alpha)}{\rho(z,\theta)} + b_1(z,\theta) \qquad (23)$$

where $b_1(z,\theta)$ is a bounded function. Then, the second term of the right hand side of (23) can be computed using a classical gauss quadrature formula. For the first term, the weak singularity is removed using a polar change variables involving ρ and α.

IV. NUMERICAL RESULTS

In this section, we present the results of the numerical simulations aiming at showing the walls effects: lateral and radial effects, on the drag force experienced by a spherical and ellipsoidal particles. Also, in the case of an ellipsoidal particle, it points out the influence of the aspect ratio, which is exploited as the orientation of the particle, in two cases: when its bigger axis is (a) along, and (b) perpendicular to the axis of the tube. We demonstrate that the drag force increases with the confinement of the flow. In order to have analogy with the Stokes force, the drag force is written as a sum of two contributions, as we already mentioned in equation (11), $i.e.$ the drag coefficient $\gamma(z)$ and the equivalent velocity field $U_{eq}(z)$. In the following, firstly, a comparison with analytical formulas of the drag force is investigated in the case of a spherical particle suspended in a cylindrical duct. Secondly, the drag coefficient on a spherical particle in a channel with a periodic changing in diameter is analyzed. The effects of the particle radius to the channel radius ratio as well as the sphere radius to the channel length ratio are carried out. Finally, we examine the influence of the aspect ratio of an ellipsoidal particle on the drag. For this purpose, let R_{p_1} and R_{p_2} be the radii of the particle along the r-axis, and the z-axis respectively, then let us introduce the following geometric parameters: ϵ=R_{p_1}/r_{min}, ψ=R_{p_2}/L and κ=R_{p_1}/R_{p_2}, where κ is equal to one in the case of a sphere and treat the variation of the drag coefficient according to these geometric parameters.

A. Case of a spherical particle

a. Comparative study: numerical vs analytical results

In order to highlight the relevance of the numerical approach even in the simplest case, $i.e$ the drag exerted on a spherical particle suspended in a Poiseuille's flow, we compare our numerical results with the analytical expansions of the coefficient γ as a function of ϵ appearing in [9]. According to this latter reference, if ϵ is small enough, then γ and U_{eq} verify:

$$\gamma/\gamma_0 = \frac{1}{1 - 2.105\epsilon + 2.087\epsilon^3}, \quad (24)$$

$$U_{eq}/U^0_{axis} = \frac{1 - 2/3\epsilon^2}{1 - 2.105\epsilon + 2.087\epsilon^3}, \quad (25)$$

where γ_0 is the Stokes drag which exerts a fluid in motion supposed to be uniform at infinity on a spherical particle, and U^0_{axis} is the incident Stokes flow along the cylinder axis. As expected, the numerical computation agrees with the expression for small ratios ϵ. In particular, the Stokes drag increases when the pore wall is closer, $i.e$, for a fixed cylinder radius, the drag force increases with the particle radius. These series expansions remain as a good approximation for a quite large ϵ ($\epsilon \leq 0.2$). Even so, for ϵ between 0.2 and 0.35 the computed drag is much more smaller than the one given by the previous expression, however when ϵ exceeds the value 0.35 the analytical drag starts to decrease. In addition, as presented in figure 4, our approach demonstrates that the drag is always an increasing function whatever the value of ϵ, in contrast to the analytical one given in [9].
In the following, we consider a channel with the sinusoidal radius variations given by Eq. (1). The studied profiles are displayed in figure 5.

b. Channel geometry and particle size effects

In this section, the minimal radius r_{min} is fixed while three different mean curvatures of the pore are considered. The drag γ and the equivalent velocity profiles U_{eq} depend on the z position of the particle. The figures 6 and 7 display these variations for two values of ϵ: $\epsilon = 0.35$ and $\epsilon = 0.7$. The maxima of γ and U_{eq} are reached at the bottle-neck of the channel while the minima of these quantities correspond to the largest radius of the pore. These results are in the same vein as for the cylindrical channel: a narrower channel leads to a larger drag. A

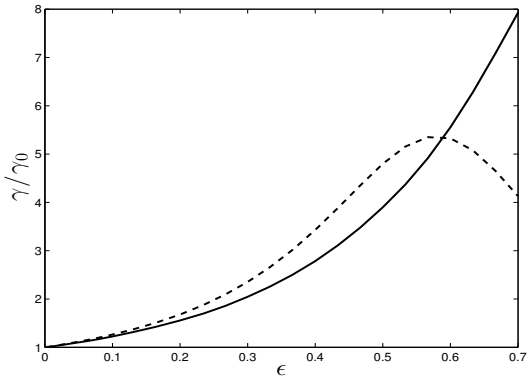

Figure 4: Comparison between numerical results represented by the solid line and analytical results represented by the dotted line. This study was performed for a cylinder of radius $R_c = 0.14$ and ϵ ranging from 0.005 to 0.7.

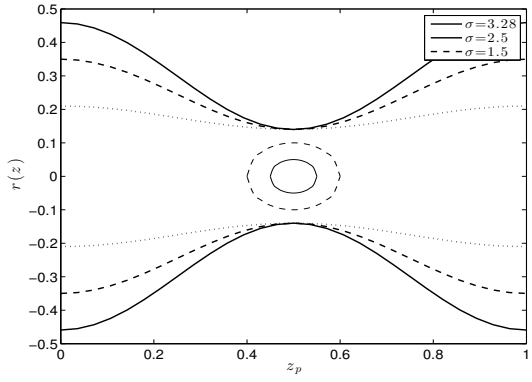

Figure 5: Pore profiles for $r_{min} = 0.14$ and three different mean curvatures $\sigma = 1.5, 2.5$ and 3.28. The circles correspond to the particles with ϵ= 0.35 and ϵ= 0.7.

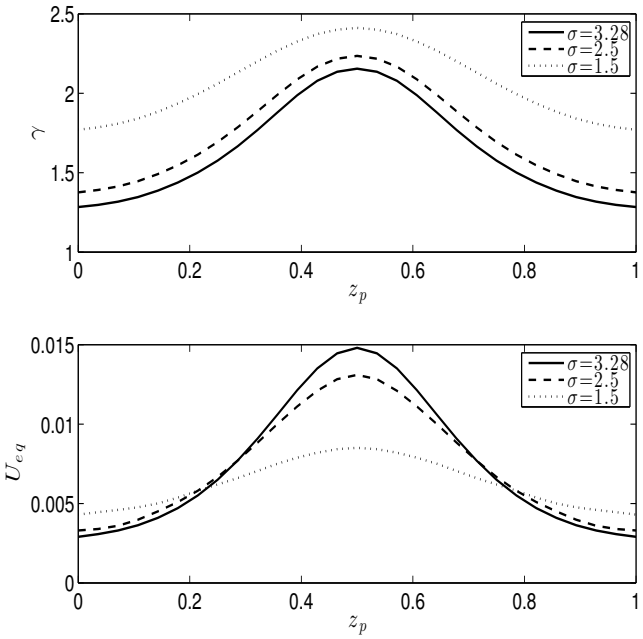

Figure 6: Spatial variation of the drag $\gamma(z)$ and the equivalent velocity field $U_{eq}(z)$ of a spherical particle with ϵ= 0.35 and ψ= 0.05. The three different pore profiles of figure 5 are considered.

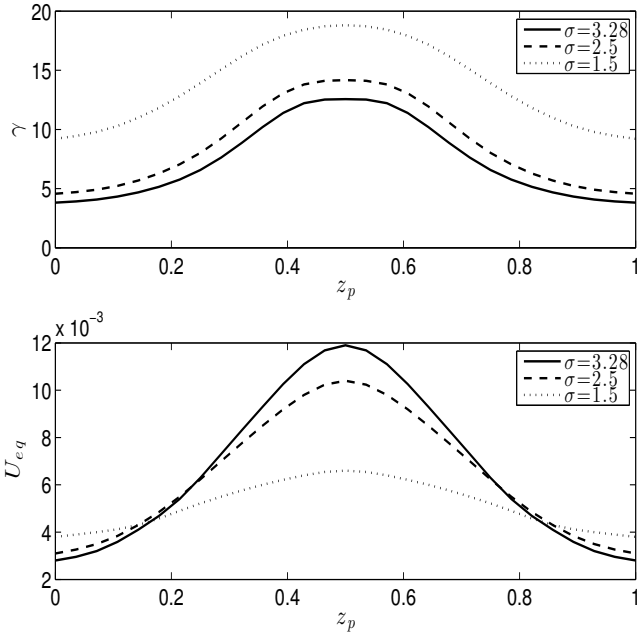

Figure 7: Spatial variation of the drag $\gamma(z)$ and the equivalent velocity field $U_{eq}(z)$ of a spherical particle with ϵ= 0.7 and ψ= 0.1. The three different pore profiles of figure 5 are considered.

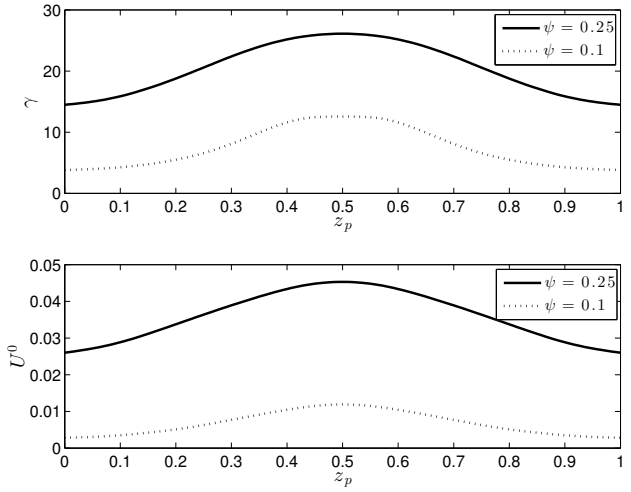

Figure 8: Spatial variation of the drag $\gamma(z)$ and the equivalent velocity field $U_{eq}(z)$ of a particle with ψ= 0.25 and ψ= 0.1. The pore profile corresponds to σ= 3.28. ϵ= 1.4 and κ = 1.

similar result arises for the equivalent velocity U_{eq}, it can be interpreted as a consequence of the fluid incompressibility assumption.
On one hand, we note that for a fixed particle radius, the relative variation of the drag increases in contrary to that of U_{eq}. In particular, let us note that the drag magnitude is constant and maximal for $\sigma = 1$ which corresponds to the case of a cylinder. For instance, for ϵ= 0.7 the drag on a particle suspended in a cylinder is equal to 25.17, this value is greater than the maximal values presented in figure 7.
On the other hand, if we compare for a same pore geometry the equivalent velocity for two different particle radii, $i.e$ two different values of ϵ, we conclude that the relative variation of the velocity is slightly smaller for larger particles. This result is expected since this velocity field corresponds to a kind of a mean effect of the fluid velocity field over the particle domain. Concerning the particle drag, its value increases dramatically with the particle radius: there is a ratio about 3 or 4 between two drags of particle of different sizes with the same pore geometry.

c. Lateral size effect

Now, we are going to examine the influence of the pore length on the drag exerted on the sphere, thereby we consider a sphere whose radius is equal to the quarter of the channel length (ψ=0.25), while in the previous section the radii were about a twentieth (ψ=0.05) and a tenth (ψ=0.1) of this latter. The other geometric parameters, σ, ϵ, and κ are always the same. If we examine the figure 8, thus we see that the drag force and the equivalent velocity for ψ=0.25 are almost three times larger than those computed where ψ=0.1.

B. Case of an ellipsoidal particle

In this final subsection, we adress the force exerted on an ellipsoidal particle, $i.e$ that the geometric parameter κ is different from 1. One should note that if κ is less than one then we say that the ellipsoidal is along the channel axis, otherwise it is perpendicular to the channel axis. Here we present the two quantities γ and U_{eq} for κ=0.5 and κ=2. Indeed, this simulation was motivated by the theory discussed in [6], demonstrating that the force exerted by the fluid varies with the orientation of the ellipsoid against the direction of the flow. We readily deduce that when the particle is perpendicular to the channel direction the intensity of the drag as well as its relative variation are much greater than when the bigger axis of the particle is oriented along the channel axis. As regards the equivalent velocity, it is slightly changed. Moreover, simulations show that if R_{p_1} changes then the drag varies significantly, while the drag is only slightly changing with the variation of R_{p2}. Indeed, for a fixed R_{p2}, we obtained a ratio which is about 2 for doubling R_{p_1}. In contrast for fixed R_{p_1} and doubling R_{p_2} the drag coefficient $\gamma(z)$ slightly changes. Furthermore, the equivalent velocity does not have a significant modification. That shows again the significant effect of the wall as in the case of the spherical particle.

C. Discussion

We discuss the results in the framework of the study of transport particle in a micropump examined in [17]. The authors point out the existence of transport mechanisms for certain parameter ranges. In order to compare our results, let us introduce the relative variation of a quantity Q, called *contrast*:

$$c_Q = \frac{Q_{max} - Q_{min}}{Q_{max} + Q_{min}}. \tag{26}$$

This contrast ranges from zero (when Q is constant) to 1 (when $Q_{min} = 0$). In the model proposed [17], the drag is assumed constant and

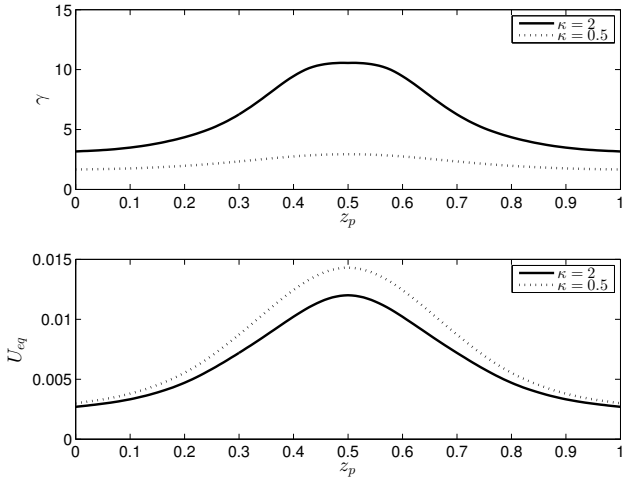

Figure 9: Spatial variation of the drag $\gamma(z)$ and the equivalent velocity field $U_{eq}(z)$ of a particle corresponding to κ= 2, ϵ= 0.7, ψ= 0.05, as well as of a particle corresponding to κ= 0.5, ϵ= 0.35, ψ= 0.1.

only the equivalent velocity varies. Thereby, they show that the particle transport may arise for a velocity contrast $c_{U_{eq}}$ about 0.6. According to figures 6 and 7 the contrasts c_γ and $c_{U_{eq}}$ increases with the curvature σ. If we compare for a same pore geometry the equivalent velocity for two different values of ϵ, then the contrast $c_{U_{eq}}$ decreases for larger particles. This result is expected since this velocity field corresponds to a kind of a mean effect of the fluid velocity field over the particle domain. Concerning the particle drag, its value increases dramatically with the particle radius: there is a ratio about 3 or 4 between two drags of particle of different sizes with the same pore geometry. We found that for a small particle $\epsilon = 0.35$, the velocity contrast varies from 0.3 to 0.66 approximatively when the pore curvature varies from 1.5 to 3.28. The drag contrast is not negligible but small about 0.1 and remains inferior to 0.18. Then, the assumption of [17] could be realized for σ about 3. If the particle size is larger ($\epsilon = 0.7$), the velocity contrast is slightly lower: its maximal value is still 0.6 for $\sigma = 3.28$. However, the drag contrast is about 0.3 and then its spatial variations are no more negligible. In addition, we find that results obtained for an ellipsoidal particle are not suitable to the transport conditions treated by [17]. Indeed, for $\kappa = 2$ and $\kappa = 0.5$ the contrast velocity was about 0.65 which could match with the transport condition, contrary to drag contrast which is equal to 0.28 for $\kappa = 0.5$ and 0.54 for $\kappa = 2$. Similar results are obtained in the case of a spherical particle with radius equal to the quarter of the pore length.

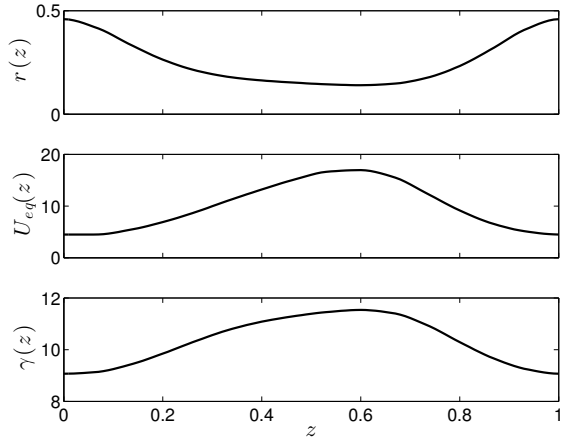

Figure 10: Pore profiles $r(z)$ and the corresponding variations of equivalent velocity field $U_{eq}(z)$ and the drag $\gamma(z)$.

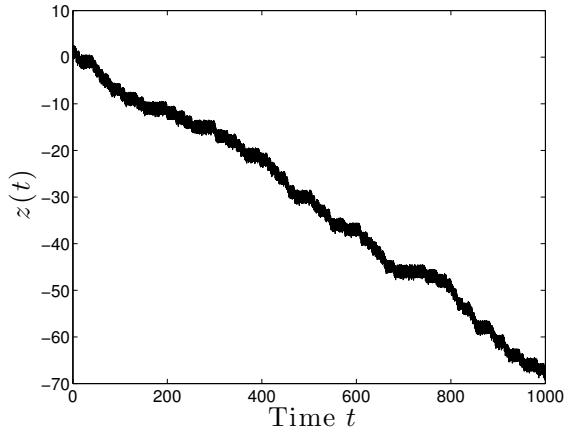

Figure 11: Particle position during 1000 periods of pumping integrated using the Eq. (27) and the drag coefficient $\gamma(z)$ and velocity field U_{eq} computed in Fig. 10.

V. APPLICATION TO PARTICLE TRANSPORT

After have discussed the variation of the drag exerted on the particle in the previous section, in the present section we focus on the dynamic of the particle especially the existence of the particle transport. According to Eq. (11) and assuming that a slow sinusoidal pumping is applied, the motion of a particle of mass m is governed by the

nonlinear differential equation:

$$m\ddot{z} = -\gamma(z)\left[\dot{z} - U_{eq}(z)\sin(2\pi t)\right] \qquad (27)$$

This equation differs from the model in [17] only by the spatial variation of γ however the equation (27) may be applied for any particle size contrary to the model in [17]. Because they showed that the transport solutions are consequence of the spatial and temporal shift symmetry and of nonlinear processes, it is expected that same mechanisms lead to a particle transport. For instance, we choose an asymmetric pore profile as displayed in figure 10 in order to have a similar velocity field to the one presented in [17]. Nevertheless, figure 10 shows that the drag force is no longer constant. For this particular value we find out a net drift to the negative value of z as appearing in figure 11. The drift velocity is small about -0.065 and intermittent: epochs of chaotic bounded dynamics alternated with fast transport to the following pores. The bifurcation scenario leading to such a transport was identified in [17] as, first, a route to chaos of the period-one solutions via a period doubling cascade. The resulting dynamics is chaotic but the strange attractor is bounded. Then by slightly varying the parameter, the strange bounded attractors merge via a crisis leading to the intermittent transport. Finally by varying the parameter, we can find a periodic transport which appears via a synchronization phenomenon as described in [26].
An analogous bifurcation analysis can be performed to find the different scenarios, but the first results show that we may expect at least the same transport solutions as found in ratchet literature. Note that a spatial variation of the inertia is known as an inertia ratchet. Here, we have a combination of a flow ratchet (due to the variation of the velocity field $U_{eq}(z)$) with the inertia ratchet.

VI. CONCLUSION

The numerical simulations reported in this paper, based on the boundary elements method, have enabled us to perform a quantitative estimation of the drag force on a spherical and ellipsoidal particles of arbitrary size in a viscous confined flow inside a periodic channel. We started by demonstrating that even in the case of a cylindrical duct, analytical approximations cannot estimate properly the drag force for particle radius larger than one-fifth of the duct radius. Thus, numerical computation of the drag force is needed. Then, we show that the drag force can be characterized by two quantities: the friction coefficient $\gamma(z)$ and the equivalent velocity field $U_{eq}(z)$. Both quantities depend on the lateral $(z - axis)$ position of the particle. We study them for different pore shapes defined by the curvature. We focus especially on their spatial variations called contrast, in order to compare with the model of particle transport used in [17]. We show that this latter model of this latter applies only for small enough particles. In the case of a spherical particle, we show how $\gamma(z)$ increases with the confinement: Nevertheless, the knowledge of γ and U_{eq} allows to get a non-linear equation of second order to describe the particle motion as in [17]. Thereby, similar system dynamical tools may be employed in order to find and understand the transport mechanisms of a particle in a periodic micropore channel. One should note, that the direct numerical simulation of such a problem was performed by [18]. However, this method increases dramatically the CPU cost comparing to our present approach. Such criterion would become crucial when long time simulation is required. That is particularly the case of the simulation of the intermittent slow transport we have presented.

References:

[1] Brenner, H.: Effect of finite boundaries on the Stokes resistance of an arbitrary particle Part 2. Asymmetrical orientations. *Journal of Fluid Mechanics*, vol. 18, no. 01: (1964) pp. 144–158.

[2] Brenner, H.: The Stokes resistance of an arbitrary particle-III Shear fields. *Chemical Engineering Science*, vol. 19, no. 09: (1964) pp. 631–651.

[3] Brenner, H.: The Stokes resistance of an arbitrary particle-IV, Arbitrary fields of flow. *Chemical Engineering Science*, vol. 19, no. 10: (1964) pp. 703–727.

[4] A.Oberbeck, Ueber stationäre Flüssigkeitsbewegunge mit Berücksichtigung der inneren Reibung, *J.reine angew.Math* 81,1876, pp. 62–80.

[5] G.Jeffery, The motion of ellipsoidal particles immersed in a viscous fluid, *Proceedings of the Royal Society A* 102,1922, pp. 161–179.

[6] S. Blaser, Forces on the surface of small ellipsoidal particles immersed in a linear flow field, *Chemical Engineering Science* 57,2002, pp. 515–526.

[7] Godin,Th. & Bouzidi, M. & Lallemand, P. & Ambari, A.: Numerical calculation of wall effect and backflow on the Stokes force. *Comptes Rendus Mécanique*, vol. 330, no. 12: (2002) pp. 837–842.

[8] Ambari, A. & Gauthier-Manuel, B. & Guyon, E.: Wall effects on a sphere translating at constant velocity. *Journal of Fluid Mechanics*, vol. 149, no. 12: (1984) pp. 235–253.

[9] Happel, J. & Byrne, B.J.: Motion of a sphere and fluid in a cylindrical tube. *Industrial & Engineering Chemistry*, vol. 46, no. 6: (1954) pp. 1181-1186.

[10] Kohr, M.: Boundary integral method for a Stokes flow past a solid sphere and a viscous drop. *Computer Methods in Applied Mechanics and Engineering*, vol. 190, no. 42: (2001) pp. 5529-5542.

[11] Schonberg, J. A. & Drew, D. A. & Belfort, G.: A neutrally buoyant sphere in creeping flow between parallel plates: farfield velocity profiles. *Chemical Engineering Science*, vol. 45, no. 1: (1990) pp. 225-235.

[12] C.Pozrikidis, Computation of Stokes flow due to the motion or presence of a particle in a tube, *Journal of Engineering Mathematics* 53,2005, pp. 1–20.

[13] Bonnet M.: Boundary integral equation methods for solids and fluids. *Wiley-Blackwell* (1999).

[14] Pozridikis, C.: Boundary integral and singularity methods for linearized viscous flow. *Cambridge University Press* (1992).

[15] Guiggiani, M. & Krishnasamy, G. & Rudolphi, T. J. & Rizzo F. J.: A general algorithm for the numerical solution of hyper singular boundary integral equations. *Journal of Applied Mechanics* vol. 59, no. 3: (1992) pp. 604–614.

[16] Kettner, Ch. & Reimann, P. & Hänggi, P. & Müller, F.: Drift Ratchet. *Phys. Rev.E* vol. 61, no. 1: (2000) pp. 312-323.

[17] Beltrame, Ph., Talkner, P. and Hänggi, P.: Deterministic transport of particles in a micro-pump. *Preprint arXiv:1205.4339*

[18] Brenk, M., Bungartz, H.-J., Mehl, M., Muntean, I. L., Neckel, T. & Weinzierl, T.: Numerical Simulation of Particle Transport in a Drift Ratchets *SIAM J. Sci. Comput.*, vol. 30: (2008) pp. 2777–2798

[19] Fedotov, V.: Numerical-analytical BEM for elliptic problems *WSEAS TRANSACTIONS on APPLIED and THERORETICAL MECHANICS*, vol. 6: (2011) pp. 131–136

[20] Etminan, A., Moosavi, M., Ghaedsharafi, N.: Determination of flow configurations and fluid forces acting on two tandem square cylinders in cross-flow and its wake patterns *INTERNATIONAL JOURNAL OF MECHANICS*, vol. 5: (2011) pp. 63–74

[21] Caraus, I., Mastorakis, NE.: The stability of collocation methods for approximate solution of singular integro-diffrential equations. *INTERNATIONAL JOURNAL on MATHEMATICS*, vol. 7: (2008) pp. 121–129

[22] Jin H, Phan-Thien N, Tanner RI, A finite element analysis of the flow past a sphere in a cylindrical tube: PTT fluid model, Computational Mechanics, 8, 409-422 (1991)

[23] Noor DZ, Chern MJ, Horng TL, An immersed boundary method to solve fluid-solid interaction problems, Computational Mechanics, 44, 447-453 (2009)

[24] Ingber MS, Mondy LA, Direct second kind boundary integral formulation for Stokes flow problems, Computational Mechanics, 11, 11-27 (1993)

[25] Chen, TC. & Skalak, R.: Stokes flow in a cylindrical tube containing a line of spheroidal particles. *Applied Scientific Research* vol. 22, no. 1: (1970) pp. 403-441.

[26] Pitkovsky, A., Rosenblum, M. and Kurths, J., Synchronization. A Universal Concept in Nonlinear Sciences, Cambridge University Press (2001)